Novel analysis technique for measuring edge density fluctuation profiles with reflectometry in the Large Helical Device

Observation of Density Fluctuations Near the Plasma Periphery with Reflectometry in LHD

A.J. Creely[1], K. Ida[2], M. Yoshinuma[2], T. Tokuzawa[2], T. Tsujimura[2], T. Akiyama[2], R. Sakamoto[2], M. Emoto[2]

[1] MIT Plasma Science and Fusion Center, Cambridge, MA, USA.
[2] National Institute for Fusion Science, Toki, Gifu, Japan.

Abstract.
    Density fluctuation profiles near the edge of LHD plasmas have been measured with reflectometry, using pellet-induced fast density scans. New work has combined local density fluctuation measurements from reflectometry with pellet-induced density scans to measure fluctuation profiles directly. Reflectometer cutoff location was calculated by proportionally scaling fast FIR density profiles to match the slower time resolution results of the ray-tracing code LHD-GAUSS. Velocity profiles generated with this reflectometer mapping were checked against velocity measurements made with CXRS, and were found to agree to within experimental uncertainty once diagnostic differences were accounted for. Measured density fluctuation profiles were found to peak strongly near the edge of the plasma, as is the case in most tokamaks. This results was confirmed with both a fixed frequency reflectometer and calibrated data from a multi-frequency comb reflectometer. The full width at half maximum of the turbulence layer near the edge of the plasma is only 2 - 3 cm, less than 5% of the normalized minor radius.

1. Introduction

Accurate measurements of density fluctuations in fusion plasmas are a key component in better understanding transport via drift wave turbulence. These measurements can be made with a variety of plasma diagnostics, including beam emission spectroscopy (BES) [1], phase contrast imaging (PCI) [2], and reflectometry [3, 4, 5]. In tokamaks, it has generally been observed that density fluctuations increase sharply toward the edge of the plasma (see [6, 7, 8, 9, 10, 11] for some examples).

This sharp increase in edge fluctuations may be due to a variety of causes. While the absolute edge density and temperature are lower than in the core, the gradients tend to be much higher, which tends to increase turbulence drive terms that go as the gradient normalized by the value [12]. In addition, there is a very sharp increase in the q profile, and thus a very rapid shift in the magnetic configuration. It is possible that this change in magnetic configuration also plays a role in the formation of edge turbulence.

In order to investigate the role of the magnetic geometry in the formation of these edge fluctuations, it is important to measure these fluctuations on devices with a variety of magnetic geometries. This motivates the measurement of fluctuations in a helical device, such as the Large Helical Device (LHD) [13, 14].

There are few experimental measurements of density fluctuation profiles in helical devices. Many local measurements of fluctuations at a single location have been made, but [15, 16] on TJ-II and [17] on Wendelstein 7AS are some of the few examples of full edge density fluctuation profile measurements on stellarators.

Previous work on LHD using inverted PCI measurements showed that the peaking of the density fluctuation profile depended heavily on the method of inversion [18, 19, 20, 21], and that some inversions led to profiles that were peaked much further in radially than is seen in typical Tokamak measurements. In order further investigate these phenomena, and avoid the use of inversions, this work aims to measure the density fluctuation profile near the edge of LHD plasmas using local measurements with a reflectometer. Since reflectometers measure fluctuations only at one radial location, profile measurements are accomplished by scanning the reflectometer cutoff location via the fast density rise and fall following a pellet injection.

This process is described in greater detail later in this paper.

Section 2 of this paper describes the various diagnostics and codes used in this study. Section 3 describes the analysis methods required to accurately map the reflectometer cutoff location and extract the fluctuation profile from the time signal. Section 4 presents the profiles and the possibility to expand these methods to future diagnostics. Section 5 presents conclusions, comparisons to past work, and motivates future work.

2. Experimental Methods

A variety of diagnostics were used in the course of this investigation. Central to all of the velocity and fluctuation measurements was the Doppler Reflectometer. Doppler reflectometry (or Doppler back-scattering) is widely used for measurements of turbulent flow velocity and amplitude [3, 4, 5]. Two types of Doppler reflectometers have been installed in LHD: a frequency-hopping system [22] and a multi-channel frequency comb system [23]. The frequency-hopping system is installed at the 9-O toroidal port (referred to as the '9-O' reflectometer) and typically set to 30.0 GHz, while the comb system is installed at the 3-O port and operates with frequencies of 27.7, 29.0, 30.5, 32.0, 33.3, 34.8, 37.0, and 38.3 GHz (referred to as the 'comb' reflectometer).

As discussed below, beyond the more simplistic estimates of the reflectometer cutoff location based solely on density profiles, a more accurate description of reflection is provided by ray tracing codes. For the basic density profiles, both Thomson Scattering [24] and FIR were used [25]. In addition, this study used the 3D ray tracing code LHD-GAUSS, which was recently upgraded and applied to electron cyclotron heating experiments in LHD [26, 27]. The code calculates ray trajectories of traveling probe waves by solving the eikonal equation under the WKB approximation. The propagation of each ray is based on the model of geometric optics with the cold plasma dispersion relation, where the electron density profile is provided by 3D equilibrium mapping of Thomson Scattering measurements [28].

Figure 1 shows examples of the ray trajectories of both Doppler reflectometer systems. The observation positions are determined by the reflection position of each ray trajectory. In this study, both reflectometers
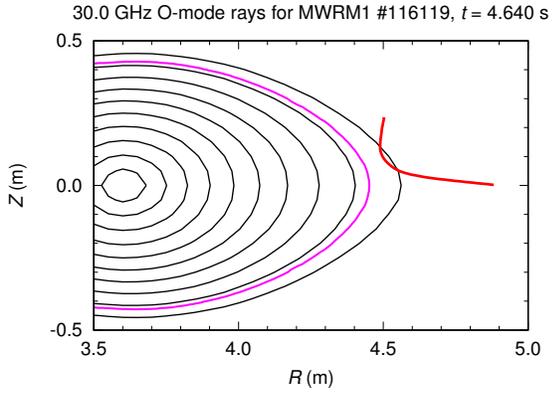
Figure 1: Examples of ray trajectory calculated by the $LHD - GAUSS$ code in a horizontal plasma cross section. The red line indicates the center ray of the probing beam. The magenta line is the nominal cutoff density, had ray tracing not been used.

operated in the ordinary mode (O-mode) polarization.

In addition to measurements with Doppler reflectometry, radial profiles of poloidal rotation velocity are measured with poloidal charge exchange spectroscopy (CXRS), using recombination emission from fully ionized carbon and the hydrogen neutral beam [29, 30]. The diagnostic has two poloidal views, one upward and one downward. The spatial pitch of the poloidal lines of sight at the mid-plane is 9mm in r_{eff} (13 mm in major radius), near the plasma edge. Since the poloidal velocity is derived from the difference in Doppler shift between the upward and downward views using three nearby channels, the effective spatial resolution is approximately 3 cm.

3. Analysis Methods

Due to the diagnostic constraints discussed above, a multi-step analysis process is required to extract the fluctuation profile from the raw reflectometer data. While each of these steps will be described in more detail later in this section, a brief summary is given here. First, in order to determine the reflection location of the reflectometer with good time resolution, inverted FIR data was used to fit density profiles at 1 ms intervals. This was then checked against slower resolution Thomson Scattering data as appropriate.

Typically, however, a density profile alone is not sufficient to determine the exact reflectometer cutoff location, since the complexities of the wave propagation in the plasma necessitate ray tracing codes [26, 27]. Running these codes at every time slice, however, tends to be prohibitively slow, and so a faster method was desired. As a fast estimate of the cutoff location, the simplistic calculation based purely on the

reflectometer frequency and density profile was redone with a cutoff density that was scaled by some constant factor, which was then checked against ray tracing results at appropriate time intervals to determine the appropriate scaling factor. The velocity profiles measured using this initial estimate and the density scan induced by the pellet injection (which radially scanned the cutoff location) were then checked against the velocity profile measured with charge exchange in order to further confirm the validity of this scaling method.

Once the cutoff density scaling has been determined using the ray tracing and velocity profile checks, the fluctuation profiles can be mapped with the more reliable cutoff location. The peak of the edge fluctuations is then used to calibrate the comb channels to the 9-O reflectometer, as these channels all have different arbitrary units, and are not pre-calibrated to one another. Once calibrated, the comb and 9-O reflectometers can be used to map out fluctuation profiles even in periods of constant density.

3.1. Profile Fitting and Reflectometer Cutoff Calculation

The first step of the fluctuation profile mapping process is the density profile fitting and cutoff location calculation. The reflectometer cutoff location must be calculated on a very fast time scale in order to resolve the fast density profile scan caused by the pellet injection. The FIR diagnostic has a very high time resolution (1ms), but low spatial resolution, while Thomson Scattering has high spatial resolution, but slow time resolution (33ms). For the purposes of this study, the fast FIR profiles were used, and were then checked against the slower Thomson profiles to ensure consistency.

FIR is inherently a line-integrated diagnostic, so the first step involved a standard inversion of the FIR line-integrated data to achieve a density profile [25]. While there are relatively few spatial data points, a simple spline fit generated a straightforward profile. This profile fit is shown in Figure 2. The spline-fit FIR profile was checked against the profile measured with Thomson Scattering at time points where the Thomson data was taken. While there are small differences between the two profiles (such as the area around Reff = 0.5 m), the two diagnostics generally agree quite well near the edge, which increases our confidence in the accuracy of the FIR profiles.
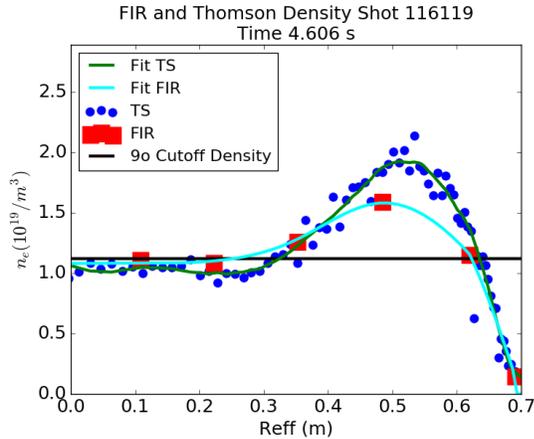
Figure 2: Density profiles measured with Thomson Scattering and FIR. Thomson Data is smoothed with a Savitzky-Golay filter, and FIR data is spline fit. Also plotted is the cutoff density corresponding to the 9-O reflectometer launch frequency.

As a first cut, the reflectometer cutoff location was then calculated as the location where the density first reached the point where the plasma frequency was equal to the reflectometer launch frequency. The time evolution of the cutoff location after the pellet injection is shown by the red trace in Figure 3. The other traces on this plot are discussed below. While obviously omitting all of the complexities of the reflectometer ray propagation, this method allows very fast calculation of the cutoff location at every 1 ms time slice, without running full ray tracing codes. In order to maintain this fast operation, while making use of more accurate ray tracing codes, the cutoff density calculated directly from the density profiles was scaled by some constant factor until the cutoff location calculated by this simple method agreed with ray tracing results at sample time slices. This process is described in the next section.

3.2. Scaling of Cutoff Density to Match Ray Tracing and CXRS

Once the density profiles have been fit and the initial calculation of the cutoff location has been completed, one can compare the cutoff location to the results of ray tracing codes in order to determine an appropriate scaling for the cutoff density. These results can then be checked by comparing the velocity profiles measured with the mapped cutoff to those measured by CXRS.
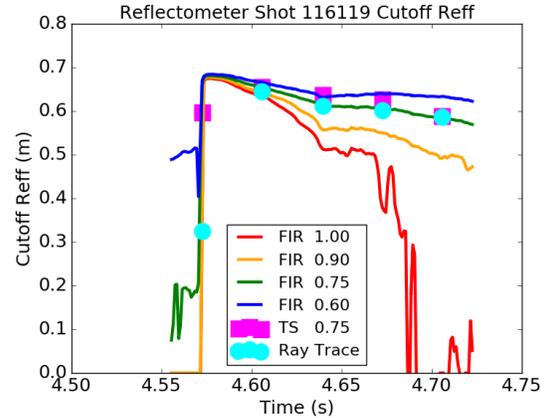

Figure 3: 9-O reflectometer cutoff location calculated via scaled cutoff densities and FIR and Thomson density profiles, checked agianst ray tracing results. FIR cutoff density scalings of 1.00 (unscaled), 0.90, 0.75, and 0.60 are shown in various colors, along with Thomson scaling of 0.75 and ray tracing calculations.

Figure 3 shows the comparison of ray tracing output with the cutoff locations calculated from FIR density profiles with different cutoff density scalings ($n_{cutoff} = Scaling \cdot n_{cutoff,1.00}$). Ray tracing was run every 33 ms, while the FIR profiles were fit every 1 ms. The different colors represent different cutoff density scalings (the factor by which the cutoff density is multiplied). For this particular shot a density cutoff scaling of approximately 0.75 achieves the best agreement with ray tracing results. While this example includes only one shot, it was observed that a scaling of between 0.7 and 0.8 worked best for most of the shots considered in this study. Figure 3 also shows a comparison with the calculations from Thomson profiles at the Thomson measurement times, also with a scaling of 0.75. The FIR and Thomson data with a scaling of 0.75 agree quite nicely with both each other and with the ray tracing calculation.

As an additional check of the accuracy of the reflectometer cutoff location, the velocity profile measured from the mapped cutoff location is now compared to the profile measured by CXRS.

As discussed before, the density scan induced by a pellet injection can be used to scan the reflectometer cutoff location, and thus map out a profile of velocity and fluctuations. As the pellet enters the plasma, the density transiently increases and then decreases. This fast change in the density profile subsequently shifts the reflectometer cutoff location outward, and then back inward. One can then back out the velocity profile by mapping the measured velocity to the location at which it was measured.

The velocity profiles mapped from a variety of cutoff scalings are shown in Figure 4.
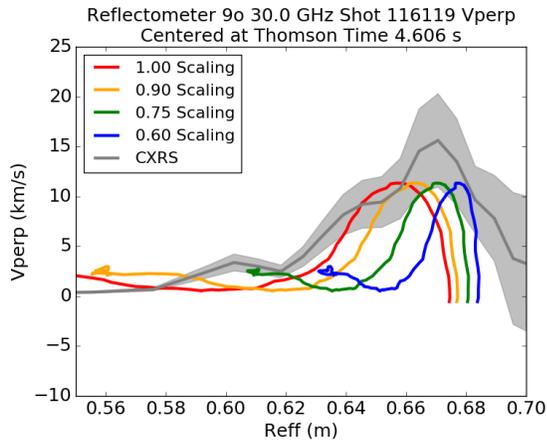
Figure 4: Perpendicular velocity profile measurements from the 9-O reflectometer and CXRS. Different colors represent different cutoff scalings for the cutoff density used to calculate the cutoff location on FIR density profiles. Diagnostic uncertainty on CXRS data is shown as the shaded grey region.

Once again, it is clear that a scaling of approximately 0.75 generates the best agreement with the location and shape of the profile measured with CXRS. The maximum magnitude differs by approximately 30%, while the overall width is very similar.

There are a number of possible causes for this slight discrepancy. First, the wave number calculation for the reflectometer has an uncertainty of approximately 20%. In addition, the velocity measured with the reflectometer is the sum of the ExB velocity and the drift wave velocity, which is approximately -2 km/s for the axes shown on the plot (the electron diamagnetic direction). Finally, the cutoff mapping procedure outlined above will certainly generate its own uncertainty. It is believed, therefore, that the slight discrepancy between the velocity profiles measured with CXRS and reflectometry are readily resolved when the above effects are taken into account. This slight discrepancy does not alter the assessment that the scaling of 0.75 agrees most closely with the CXRS measurements. More precise uncertainty quantification for this new diagnostic technique will be addressed in future work.

As is expected, the inner side of the profile seems to be more accurate than the outer (core rather than scrape-off-layer), since the reflectometer measurements will be much less reliable outside of the last closed flux surface.

While a more quantitative comparison of the velocity profiles is beyond the scope of this study, the general agreement in profile shape, and the close agreement with the overall profile once the cutoff density has been scaled, indicates that the

pellet-induced density scans allow accurate profile measurements with the reflectometer, and that the same method can likely be applied to density fluctuation measurements.

3.3. Calibration of Comb Reflectometer

In addition to using the density scan to compare to CXRS in order to determine the appropriate cutoff density scaling, this scan can also be used to calibrate the multi-channel comb reflectometer against the single channel 9-O reflectometer. The 9-O reflectometer velocity measurements are calibrated to measure in km/s directly. The comb reflectometer, however, measures velocity in arbitrary units, which are also different for each channel. This means that without some type of cross-calibration, channels cannot be compared to one another, or to the 9-O reflectometer.
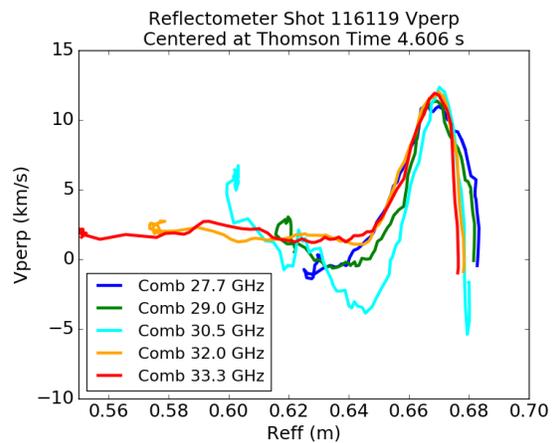

Figure 5: Perpendicular velocity profiles measured with five channels of the comb reflectometer. A cutoff density scaling of 0.75 was used. Calibrated to the 9-O measurement.

The pellet-induced density scan can be used for just such a calibration. The profiles measured by all of the comb channels can be plotted on top of the 9-O profile, and then calibrated such that the profiles agree as closely as possible. The same cutoff density scaling is used as for the 9-O reflectometer. Figure 5 shows the calibrated comb channels. Three comb channels were not operational in this shot, and are therefore omitted from the figure. These profiles also agree quite closely with that measured with the 9-O reflectometer, shown in Figure 4.

Once this calibration has been completed, one can then compare the different channels directly at other times in the shot. This enables profile measurements even when at time periods with constant density.

More importantly, a similar procedure can be applied to the fluctuation profiles, described in the

next section, which allows measurement of fluctuation profiles at all times in the shot.

4. Density Fluctuation Profiles

Once the reflectometer cutoff location has been calculated, scaled appropriately, and the comb reflectometer has been calibrated to the 9-O reflectometer, one can use the pellet-induced density scan to measure the density fluctuation profiles in the same manner as the velocity profiles.

As reference, the temperature and density profiles in the plasma for which the fluctuations were measured are shown in Figure 6.

4.1. Fluctuation Profile from 9-O Reflectometer

Figure 7 shows the density fluctuation profiles for three different frequency ranges measured by the 9-O reflectometer after a pellet injection. This figure shows that the fluctuations are strongly peaked near the edge in all frequency ranges, though the lowest frequency range may contain signals from MHD activity, which is not the primary focus of this study.

This profile agrees roughly with some of the PCI inversions in [21], which shows a strong peak right near the edge of the plasma, while disagreeing significantly with other inversions. In addition, this profile agrees generally with the edge peaking seen in tokamaks. PCI inversions have not yet been completed for this shot, and such comparisons will be the subject of future work.

In both this shot and others, the radial width of the fluctuation feature seems to be largest for the 30 -150 kHz range (2-3 cm full width at half-maximum), with a decreasing width at higher frequencies. Further investigation of this turbulent feature width will be the subject of future work.
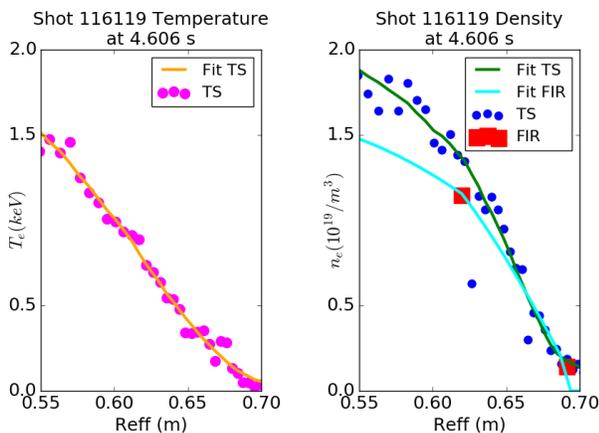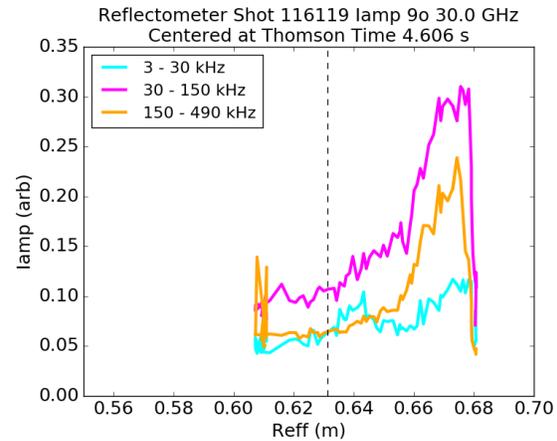

Figure 7: Density fluctuations measured with the pellet-induced density scan and the 9-O reflectometer in three frequency ranges. The lowest frequency range may contain some signal from MHD events. Vertical dotted line is a99.

4.2. Fluctuation Profile from Comb Reflectometer

In addition to the 9-O reflectometer, the edge density fluctuation profile was also measured with the comb channels. As with the velocity measurements, the comb density fluctuation measurements all use arbitrary units, and each channel uses different arbitrary units. The comb reflectometer must therefore be calibrated to the 9-O reflectometer using the same method that was used for the velocity measurements.

Figure 8 shows the calibrated comb measurements. Again, there are three comb channels that were not operating properly in this shot, which are omitted from

Figure 6: Temperature and density profiles for the shot analyzed in this study. Raw data and fits both shown.
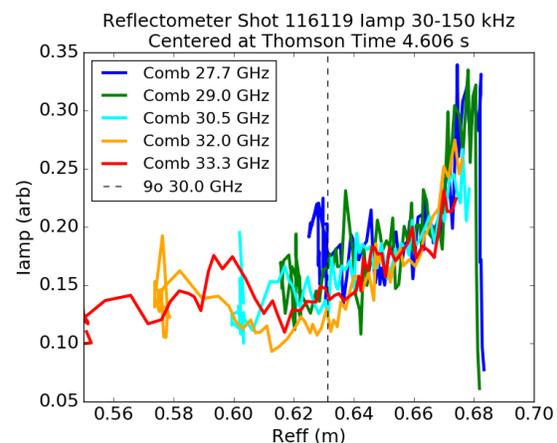

Figure 8: Density fluctuations in the 30 - 150 kHz range measured with the pellet-induced density scan and five channels of the comb reflectometer. A cutoff density scaling of 0.75 was used. Calibrated to the 9-O measurement. Vertical dotted line is a99.

this figure. While the agreement for the fluctuation profile is not as clean as for the velocity profile, the various channels clearly show a very similar profile shape and location. There is some discrepancy in the inner radii, but this may have to do with the noise floor for the comb channels, which is higher than for the 9-O reflectometer.

A more detailed calibration of the comb reflectometer and application to other time periods in the shot, in addition to the pellet injection, will be addressed in future work.

5. Conclusions

This work has outlined a new method of measuring density fluctuation profiles on LHD using a pellet-induced density scan and reflectometry. Fast density profiles are measured with 1ms time resolution using the FIR diagnostic. The cutoff location of the reflectometer is then calculated using a scaled cutoff density which is matched to ray tracing codes for accuracy. The fast cutoff mapping then enables fast density scans caused by pellet injections to measure velocity and density fluctuation profiles. Velocity profiles agree qualitatively with CXRS results, and may agree quantitatively when the k-spectrum and uncertainty in the mapping location is taken into account.

The measured density fluctuation profiles are strongly peaked near the edge of the plasma, as is seen on many tokamaks [6, 7, 8, 9, 10, 11] and other helical devices [15, 16, 17]. The full width at half maximum of the turbulence layer near the edge is only 2 - 3 cm, less than 5% of the normalized minor radius.

The results of this study suggest that the spatial resolution of PCI (typically 10 to 50% of the normalized minor radius, depending on the inversion method and the spectrum of turbulence wave numbers [21]) is insufficient to study the radial structure of density fluctuations which are highly localized near the plasma edge.

In the future, this technique will be applied to a much larger variety of shots, and proper calibration of the comb channels will enable measurement at times other than the pellet injection itself. Fluctuation profiles measured with PCI and reflectometry will also be compared from the same shot. Finally, the uncertainty in these measurements will be better quantified. It is also possible that such a technique may be able to inform gyrokinetic simulations of stellarator plasmas, if the plasma density or reflectometer frequency is chosen such that the cutoff is closer to the core of the plasma.

6. Acknowledgements

7. References

[1] Mandl, W. et al., Plasma Phys. Control. Fusion 35, 1373 (1993).
[2] Weisen, H. Infrared Phys. 25 (3), 543-549 (1985).
[3] Hirsch, M. et al., Plasma Phys. Control. Fusion 43, 1641 (2001).
[4] Conway, G.D. et al., Plasma Phys. Control. Fusion 46, 951 (2004).
[5] Tokuzawa, T. et al., Rev. Sci. Instrum. 83, 10E322 (2012).
[6] Hanson, G.R. et al., Nucl. Fusion 32, 1593 (1992).
[7] Sabot, R. et al. Plasma Phys. Control. Fusion 48, B421B432 (2006).
[8] McKee, G. R. et al., Plasma Fusion Res. 2, S1025 (2007).
[9] Yan, Z. et al. Phys. Rev. Lett. 107, 055004 (2011).
[10] Groebner, R.J. et al., Nucl. Fusion 53, 093024 (2013).
[11] Stroth, U. et al., Nucl. Fusion 55, 083027 (2015).
[12] Kotschenreuther, M. et al., Phys. Plasmas 2, 2381 (1995).
[13] Fujiwara, M. et al., Nucl. Fusion 41 (10), 1355 (2001).
[14] Motojima, O. et al., Nucl. Fusion 43, 1674 (2003).
[15] Saffman, M. et al., Rev. Sci. Instrum. 72 (6), 2579 (2001).
[16] Basse, N.P. et al., Plasma Sources Sci. Technol. 11, A138A142 (2002).
[17] Happel, T. Doppler Reflectometry in the TJ-II Stellarator: Design of an Optimized Doppler Reflectometer and its Application to Turbulence and Radial Electric Field Studies. PhD Thesis, Universidad Carlos III de Madrid (2010).
[18] Tanaka, K. et al., Rev. Sci. Instrum. 74 (3), 1633 (2003).
[19] Tanaka, K. et al., Rev. Sci. Instrum. 79, 10E702 (2007).
[20] Michael, C.A. et al., Plasma Fusion Res. 3, S1071 (2008).
[21] Michael, C.A. et al., Rev. Sci. Instrum. 86, 093503 (2015).
[22] Tokuzawa, T. et al., Rev. Sci. Instrum. 81, 10D906 (2008).
[23] Tokuzawa, T. et al., Plasma Fusion Res. 9, 1402149 (2014).
[24] Yamada, I. et al., JINST 7, C05007 (2012).
[25] Kawahata, K. et al., Fusion Eng. Des. 34, 393 (1997).
[26] Kubo, S. et al., AIP Conf. Proc. 669, 187 (2003).
[27] Tsujimura, T. Ii et al., Nucl. Fusion 55, 123019 (2015).
[28] Suzuki, C. et al., Plasma Phys. Control. Fusion 55, 014016 (2013).
[29] Ida, K. et al., Rev. Sci. Instrum. 71 (6), 2360 (2000).
[30] Yoshinuma, M. et al., Fusion Sci. Technol. 58, 375 (2010) .